Structural Properties of Docosahexaenoyl Phospholipid Bilayers Investigated by Solid-State ^{2}H NMR Spectroscopy

Horia I. Petrache,[†,§] Amir Salmon,[‡] and Michael F. Brown*[,‡]

Contribution from the Department of Physiology, Johns Hopkins University School of Medicine, Baltimore, Maryland 21205, and Department of Chemistry, University of Arizona, Tucson, Arizona 85721

Received July 17, 2001

Abstract: Polyunsaturated lipids in cellular membranes are known to play key roles in such diverse biological processes as vision, neuronal signaling, and apoptosis. One hypothesis is that polyunsaturated lipids are involved in second messenger functions in biological signaling. Another current hypothesis affirms that the functional role of polyunsaturated lipids relies on their ability to modulate physical properties of the lipid bilayer. The present research has employed solid-state ^{2}H NMR spectroscopy to acquire knowledge of the molecular organization and material properties of polyunsaturated lipid bilayers. We report measurements for a homologous series of mixed-chain phosphatidylcholines containing a perdeuterated, saturated acyl chain (*n*:0) at the *sn*-1 position, adjacent to docosahexaenoic acid (DHA, 22:6ω3) at the *sn*-2 position. Measurements have been performed on fluid (L_α)-state multilamellar dispersions as a function of temperature for saturated acyl chain lengths of $n = 12$, 14, 16, and 18 carbons. The saturated *sn*-1 chains are therefore used as an intrinsic probe with site-specific resolution of the polyunsaturated bilayer structure. The ^{2}H NMR order parameters as a function of acyl position (order profiles) have been analyzed using a mean-torque potential model for the chain segments, and the results are discussed in comparison with the homologous series of disaturated lipid bilayers. At a given absolute temperature, as the *sn*-1 acyl length adjacent to the *sn*-2 DHA chain is greater, the order of the initial chain segments increases, whereas that of the end segments decreases, in marked contrast with the corresponding disaturated series. For the latter, the order of the end segments is practically constant with acyl length, thus revealing a universal chain packing profile. We find that the DHA-containing series, while more complex, is still characterized by a universal chain packing profile, which is shifted relative to the homologous saturated series. Moreover, we show how introduction of DHA chains translates the order profile along the saturated chains, making more disordered states accessible within the bilayer central region. As a result, the area per lipid headgroup is increased as compared to disaturated bilayers. The systematic analysis of the ^{2}H NMR data provides a basis for studies of lipid interactions with integral membrane proteins, for instance in relation to characteristic biological functions of highly unsaturated lipid membranes.

Introduction

Docosahexaenoic acid (DHA, 22:6ω3) is the most unsaturated fatty acid commonly present in biological membranes. Large quantities of polyunsaturated lipids, especially DHA, are found in the brain gray matter and synaptic membranes.[1,2] In particular, the outer segment membranes of the rod cells of the retina contain close to 50 mol % DHA of the total fatty acid components.[3,4] Evidence for a functional role of DHA lipids has been accumulating from various physiological studies. For example, biological effects of polyunsaturated fatty acids (PUFAs) such as DHA on neural processes have been investigated through dietary manipulations of the ω3 essential fatty acid (EFA) precursor, α-linolenic acid (18:3ω3), in rats[5,6] and monkeys.[7] It has been observed that a dietary reduction in ω3 PUFA content involving DHA is compensated by a concomitant increase in ω6 PUFAs such as DPA (docosapentaenoic acid, 22:5ω6), although significant alterations of function still occur. In humans, the influence of DHA in nervous system development has been studied by Uauy et al.,[8] who showed reduced learning ability and significant visual disfunction of human infants who were fed formulas with reduced DHA content. These studies linked the high levels of DHA found in human placental blood and breast milk with the need for preformed DHA in infant development. Consequently, there is increased emphasis on supplementation of human infant formulas with preformed DHA.[9−11] DHA has also been shown to be involved

* Corresponding author. Tel.: 520-621-2163. Fax: 520-621-8407. E-mail: mfbrown@u.arizona.edu.

[†] Johns Hopkins University School of Medicine.

[‡] University of Arizona.

[§] Current address: Laboratory of Physical and Structural Biology, NICHD, National Institutes of Health, Bethesda, MD 20892.

(1) Salem, N.; Kim, H. Y.; Yergey, J. A. In *Health Effects of Polyunsaturated Fatty Acids in Seafoods*; Simopoulos, A. P., Kifer, R. R., Martin, R. E., Eds; Academic Press: New York, 1986; pp 263−317.

(2) Salem, N.; Wegher, B.; Mena, P.; Uauy, R. *Proc. Natl. Acad. Sci. U.S.A.* **1996**, *93*, 49−54.

(3) Stone, W. L.; Fransworth, C. C.; Dratz, E. A. *Exp. Eye. Res.* **1979**, *28*, 387−397.

(4) Brown, M. F. *Curr. Top. Membr.* **1997**, *44*, 285−356.

(5) Bouree, J. M.; Durand, G.; Pascal, G.; Youyou, A. *J. Nutr.* **1989**, *119*, 15−22.

(6) Greiner, R. S.; Moriguchi, T.; Hutton, A.; Slotnick, B. M.; Salem, N. *Lipids* **1999**, *34*, S239−S243.

(7) Neuringer, M.; Connor, W. E.; Lin, D. S.; Barstad, L.; Luck, S. *Proc. Natl. Acad. Sci. U.S.A.* **1986**, *83*, 4021−4025.

(8) Uauy, R.; Peirano, P.; Hoffman, D.; Mena, P.; Birch, D.; Birch, E. *Lipids* **1996**, *31*, S167−S176.

(9) Neuringer, M. *Am. J. Clin. Nutr.* **2000**, *71*, 256S−267S.

10.1021/ja011745n CCC: $20.00
Published on Web 11/17/2001

in human diseases as diverse as cancer, cystic fibrosis, and multiple sclerosis (see Stillwell[12] and Jenski[13] for recent reviews).

One interesting aspect is that the mammalian organism goes to a long extent to produce and maintain high concentrations of DHA.[14] In particular, mammals must obtain the associated essential fatty acid precursor 18:3ω3 from their diet in order to form DHA through a series of enzymatic reactions involving elongases and desaturases.[2] In addition, the susceptibility to autooxidative damage necessitates large amounts of vitamin E (α-tocopherol) to prevent degradation of DHA,[15] again consistent with an essential biological role of PUFAs.[14] However, the exact mechanisms of action of PUFAs are still largely unknown. One possibility is that PUFAs act as ligands for receptors involved in transcription[16] or biological signaling.[1,17−20] Yet the large concentration of PUFA-lipids found in the brain and retina is difficult to explain by such a mechanism. An alternative hypothesis is that PUFAs yield characteristic membrane properties associated with lipid−protein interactions.[21−23] In agreement with the second hypothesis, measurements using flash photolysis have suggested that the bulk properties of DHA-containing phospholipids are required for proper photoactivity of the G protein-coupled receptor, rhodopsin.[23,24] These properties may include the elastic curvature stress of the membrane coupled to the activation of the receptor protein, and subsequent signal transduction.[23] The above observations have led to a renewed interest in the biophysical properties (structure in particular) of polyunsaturated bilayers.[14,23,25−29] Knowledge of structural properties enhances our understanding of molecular level interactions between lipid molecules themselves, as well as with protein components, because these interactions are reflected in the intimate molecular packing within the cell membrane.[30−33]

The structural and dynamical properties of polyunsaturated chains are revealed by comparison with saturated bilayers, as demonstrated by Salmon et al.,[30] who contrasted the ^{2}H NMR spectrum of (16:0-d_{31})(22:6)PC with that of di(16:0-d_{31})PC lipid bilayers in the fluid (L_α) state. The differences in the ^{2}H NMR spectra were interpreted in terms of an increase in the configurational freedom of the palmitoyl (16:0) chains due to the adjacent DHA chain. A more extensive ^{2}H NMR analysis was performed by Barry et al.[34] for the homologous series of mixed-chain, polyunsaturated (n:0-d_{2n-1})(22:6) phosphatidylcholines, with n = 12, 14, 16, and 18 carbons, in comparison with the homologous series of the corresponding symmetric lipids, di(m:0-d_{2m-1}) phosphatidylcholines. By contrasting the features of the two homologous series, rather than individual lipids, one has a qualitative gain in understanding the effect of polyunsaturation on the bilayer dynamic structure. An alternative route to investigate the effects of polyunsaturation has been undertaken by Holte et al.,[25,26] who compared lipids with different levels of unsaturation in the *sn*-2 position, for a fixed *sn*-1 chain (18:0-d_{35}) labeled for ^{2}H NMR spectroscopy. From this perspective, using a mixed-chain, unsaturated series of stearoyl phosphatidylcholines, Holte et al.[25,26] showed that the ^{2}H NMR spectra of the saturated perdeuterated (18:0-d_{35}) chain changed markedly with the nature of the *sn*-2 chain, and consequently that the order parameter profile changed shape, with significant perturbation in the midchain region.

In this paper, we follow the approach of Barry et al.[34] and compare bilayers of the polyunsaturated series (n:0-d_{2n-1})-(22:6)PC with the disaturated series of di(m:0-d_{2m-1}) phosphatidylcholines. Here we focus on the detailed structural properties of polyunsaturated lipid bilayers in the liquid-crystalline (L_α) state. We have previously investigated[35] the homologous series of disaturated phosphatidylcholines, di(m:0)PC in the L_α phase, and shown how the ^{2}H NMR measurements can be interpreted using a statistical model for the acyl chain configurational disorder. The present study represents a natural extension to the case of mixed-chain, saturated−polyunsaturated bilayers, in which influences of polyunsaturation on the bilayer physical properties have been systematically explored using ^{2}H NMR spectroscopy. By doing so, we discovered a number of interesting new aspects. First, as shown by Salmon et al.[30] for the case of (16:0)(22:6)PC in the fluid state, polyunsaturation at the glycerol *sn*-2 position increases the *sn*-1 chain disorder for all mixed-chain lipids in the series. This leads to an increased cross-sectional area (lower surface density) and reduced hydrocarbon thickness when compared to their disaturated counterparts at a given absolute temperature. A second important aspect is that, at fixed absolute temperature, longer *sn*-1 chains show *decreased* order at the chain end (bilayer center) but *increased* order in the vicinity of the lipid headgroups. Despite this complex behavior, we find a universal chain packing curve for the mixed-chain saturated−polyunsaturated bilayers, just as previously obtained for the disaturated series.[35] By comparing the packing profiles, we are able to show how the DHA chain affects the overall chain packing within the bilayer. Finally, the detailed structural results that emerge from this systematic analysis of ^{2}H NMR data provide a firm conceptual framework for studies

(10) Uauy, R.; Mena, P.; Rojas, C. *Proc. Nutr. Soc.* **2000**, *59*, 3−15.
(11) Jorgensen, M. H.; Hernell, O.; Hughes, E. L.; Michaelsen, K. F. *J. Ped. Gastro. Nutr.* **2001**, *32*, 293−296.
(12) Stillwell, W. *Curr. Org. Chem.* **2000**, *4*, 1169−1183.
(13) Jenski, L. J. *Curr. Org. Chem.* **2000**, *4*, 1185−1200.
(14) Bloom, M.; Linseisen, F.; Lloyd-Smith, J.; Crawford, M. In *Magnetic Resonance and Brain Function: Approaches from Physics*; Maraviglia, B., Ed.; IOS Press: Amsterdam, 1999; pp 527−553.
(15) Kelley, E. E.; Buettner, G. R.; Burns, C. P. *Arch. Biochem. Biophys.* **1995**, *319*, 102−109.
(16) de Urquiza, A. M.; Liu, S. Y.; Sjoberg, M.; Zetterstrom, R. H.; Griffiths, W.; Sjovall, J.; Perlmann, T. *Science* **2000**, *290*, 2140−2144.
(17) Albino, A. P.; Juan, G.; Traganos, F.; Reinhart, L.; Connolli, J.; Rose, D. P.; Darzynkiewicz, Z. *Cancer Res.* **2000**, *60*, 4139−4145.
(18) Chen, Z. Y.; Istfan, N. W. *Prostaglandins, Leukotrienes Essent. Fatty Acids* **2000**, *63*, 301−308.
(19) Siddiqui, R. A.; Jenski, L. J.; Neff, K.; Harvey, K.; Kovacs, R. J.; Stillwell, W. *Biochim. Biophys. Acta* **2001**, *1499*, 265−275.
(20) Kim, H. Y.; Akbar, M.; Lau, A.; Edsall, L. *J. Biol. Chem.* **2000**, *275*, 35215−35223.
(21) Gibson, N. J.; Brown, M. F. *Biochem. Biophys. Res. Commun.* **1990**, *169*, 1028−1034.
(22) Mitchell, D. C.; Straume, M.; Litman, B. J. *Biochemistry* **1992**, *31*, 662−670.
(23) Brown, M. F. *Chem. Phys. Lipids* **1994**, *74*, 159−180.
(24) Liebman, P. A.; Botelho, A. V.; Brown, M. F.; Parkes, J. H. *Biophys. J.* **2001**, *80*, 244.
(25) Holte, L. L.; Peter, S. A.; Sinnwell, T. M.; Gawrisch, K. *Biophys. J.* **1995**, *68*, 2396−2403.
(26) Holte, L. L.; Separovic, F.; Gawrisch, K. *Lipids* **1996**, *31*, S199−S203.
(27) Litman, B. J.; Mitchell, D. C. *Lipids* **1996**, *31*, S193−S197.
(28) Huster, D.; Jin, A. J.; Arnold, K.; Gawrisch, K. *Biophys. J.* **1997**, *73*, 855−864.
(29) Huster, D.; Arnold, K.; Gawrisch, K. *Biochemistry* **1998**, *37*, 17299−17308.
(30) Salmon, A.; Dodd, S. W.; Williams, G. D.; Beach, J. M.; Brown, M. F. *J. Am. Chem. Soc.* **1987**, *109*, 2600−2609.
(31) Bloom, M. J.; Evans, E.; Mouritsen, O. G. *Q. Rev. Biophys.* **1991**, *24*, 293−397.
(32) Petrache, H. I.; Grossfield, A.; MacKenzie, K. R.; Engelman, D. M.; Woolf, T. B. *J. Mol. Biol.* **2000**, *302*, 727−746.
(33) Petrache, H. I.; Zuckerman, D. M.; Sachs, J. N.; Killian, J. A.; Koeppe, R. E.; Woolf, T. B. *Langmuir*, in press.
(34) Barry, J. A.; Trouard, T. P.; Salmon, A.; Brown, M. F. *Biochemistry* **1991**, *30*, 8386−8394.
(35) Petrache, H. I.; Dodd, S. W.; Brown, M. F. *Biophys. J.* **2000**, *79*, 3172−3192.

of lipid interactions with integral membrane proteins, including G-protein coupled receptors such as rhodopsin.

Methods

Experimental Procedures. Polyunsaturated phospholipids (n:0-d_{2n-1})(22:6)PC, with $n = 12$, 14, 16, and 18 carbons, were synthesized as described.[30] Perdeuteration of fatty acids (Sigma, St. Louis, MO) was performed with ^2H gas using a 10% Pd−charcoal catalyst. The docosahexaenoic acid was purchased from Nu Chek Prep. Inc. (Elysian, MN) and used without further purification. Disaturated phospholipids were synthesized from the perdeuterated fatty acid anhydrides and the cadmium chloride adduct of *sn*-glycero-3-phosphocholine,[36] and then purified on silica gel columns. Next, the *sn*-2 chains of the disaturated lipids were hydrolyzed with snake venom phospholipase A_2 from *Crotalus adamanteus* (Sigma, St. Louis, MO). The resulting lysophospholipid was reacylated with the anhydride of docosahexaenoic acid to obtain the mixed-chain phospholipids, followed by silica gel chromatography. The docosahexaenoic acid-containing samples were all handled under argon with use of solvents containing butylated hydroxytoluene (BHT) as an antioxidant (in a molar proportion of 0.1% BHT to phospholipid). Treatment of the samples with phospholipase A_2, followed by transesterification of the released *sn*-2 fatty acids and gas−liquid chromatography, detected less than 2% acyl chain migration. This indicated a high isomeric purity of the product phospholipid. NMR samples were prepared as 50 wt % multilamellar dispersions of 200−250 mg of lipid in 67 mM sodium phosphate buffer, pH 7.0, using ^2H-depleted water (Aldrich). Samples were stored under argon at −80 °C while not in use. Solid-state ^2H NMR spectra were acquired at 55.43 MHz as described,[34,35] and measurements were made for each lipid as a function of temperature. The temperature was controlled within ±0.5 °C. All samples were subsequently checked by thin-layer chromatography, and revealed no contamination or degradation.

The ^2H NMR spectral powder patterns were numerically deconvoluted (de-Paked) to yield the $\theta = 0°$ oriented spectra, as described by Bloom et al.[37] Peak assignments were made with the assumptions that the order parameters decrease in magnitude from C_2 (α carbon) to the methyl end, and that the area under each peak is proportional to the number of deuterons generating the peak.[36] The C−^2H bond order parameters, $S_{CD}^{(i)}$ of the de-Paked ^2H NMR spectra were calculated from the quadrupolar splittings using the relation[38]

$$|\Delta\nu_Q| = \frac{3}{2}\chi_Q|S_{CD}^{(i)}||P_2(\cos\theta)| \tag{1}$$

where $\chi_Q \equiv e^2qQ/h = 167$ kHz,[39] θ represents the angle between the bilayer director axis and the static magnetic field direction, and $P_2(\cos\theta) = (3\cos^2\theta - 1)/2$, which for $\theta = 0°$ is equal to unity. The quadrupolar splitting is designated as $(\Delta\nu_Q)_\parallel$ for the bilayer normal parallel to the main magnetic field ($\theta = 0°$), and $(\Delta\nu_Q)_\perp$ for the perpendicular orientation ($\theta = 90°$). Based on geometrical considerations, the values of $S_{CD}^{(i)}$ are assumed to be negative.

Mean-Torque Model of Segmental Conformations. Before presenting the structural results, we briefly summarize the theoretical considerations of the acyl chain configurational properties. The S_{CD} observables from ^2H NMR spectroscopy represent a measure of the carbon−deuterium (CD) bond orientations with respect to the static external magnetic field axis.[38] The order parameter $S_{CD}^{(i)}$ of carbon segment (i) is essentially the ensemble average $\langle 3\cos^2\beta^{(i)} - 1\rangle/2$, where $\beta^{(i)}$ denotes the angle between the C−^2H bond direction (principal axis frame) and the bilayer normal (director axis), and the brackets indicate a time or ensemble average. As discussed elsewhere,[35,40] the conversion of the order parameters into structural quantities, such as acyl chain length, requires a model for the segmental motions to calculate the average $\langle\cos\beta^{(i)}\rangle$ from the value of $\langle\cos^2\beta^{(i)}\rangle$. For this, one needs to consider the distribution function $f(\cos\beta^{(i)})$ that gives the relative populations of all possible tilt angles $\beta^{(i)}$.[35,40,41] The conventional approach is based on a diamond lattice representation of chain conformations,[42] which gives the segmental projection along the bilayer normal as[43,44]

$$\langle\cos\beta^{(i)}\rangle = 1/2 - S_{CD}^{(i)} \tag{2}$$

A more recent result[35,41] uses a continuum description of segmental orientations and, for $|S_{CD}^{(i)}| > 1/8$ gives

$$\langle\cos\beta^{(i)}\rangle = \frac{1}{2}\left(1 + \sqrt{\frac{-8S_{CD}^{(i)} - 1}{3}}\right) \tag{3}$$

(For $|S_{CD}^{(i)}| < 1/8$, numerical calculations are needed as discussed previously.[35,41]) This expression has been shown to be superior to the diamond lattice model based on molecular dynamics simulations.[41,45]

In the framework of this continuum model, segmental orientations are described using a mean-field potential $U(\beta)$, which is the generator of the segmental distribution function $f(\beta)$ according to

$$f(\beta) = \frac{1}{Z}\exp\left(-\frac{U(\beta)}{k_BT}\right) \tag{4}$$

with the partition function Z being given by

$$Z = \int_0^\pi \exp\left(-\frac{U(\beta)}{k_BT}\right)\sin\beta\,d\beta \tag{5}$$

Here the carbon index i has been suppressed for clarity. The mean-field potential $U(\beta)$ (called the potential of mean torque) is determined empirically from the experimentally measured order parameters S_{CD}. In a first-order approximation, it can be written as

$$U(\beta) \approx -k_BT\epsilon_1\cos\beta \tag{6}$$

where ϵ_1 is a dimensionless model parameter which quantifies the orientational confinement of the acyl segment in k_BT energy units.[35] Note that the potential of mean torque is an odd function of the segment tilt because it changes sign upon inversion. The advantage of the first-order mean-torque model is that it allows conversion of the order parameter profiles $S_{CD}^{(i)}$ into an equivalent mean-torque parameter (mean-torque strength) profile, given by the $\epsilon_1^{(i)}$ values as a function of acyl chain segment index i. In what follows, we apply the first-order mean-torque model to the ^2H NMR order parameters of the saturated chains of the mixed-chain lipids, viz. (n:0-d_{2n-1})(22:6) phosphatidylcholines, to calculate average structural parameters.

Calculation of Structural Parameters. For planar bilayers, the main structural parameters of interest are the average cross-sectional area of the acyl chain $\langle A_C\rangle$ and the average acyl chain length L_C, which are defined and calculated as explained.[35] In the present case we are interested in comparing the properties of the mixed-chain, saturated−polyunsaturated PC series to the corresponding disaturated series, based on measurements on the saturated *sn*-1 chain. For the plateau region, assuming that the saturated segmental cross-sectional area and the projected length are inversely correlated,[38,40,41] we have that

(36) Williams, G. D.; Beach, J. M.; Dodd, S. W.; Brown, M. F. *J. Am. Chem. Soc.* **1985**, *24*, 6868−6873.
(37) Bloom, M.; Davis, J. H.; MacKay, A. L. *Chem. Phys. Lett.* **1981**, *80*, 198−202.
(38) Brown, M. F. In *Biological Membranes*; Merz, K. M., Roux, B., Eds.; Birkhäuser: Boston, 1996; pp 175−252.
(39) Davis, J. H. *Biochim. Biophys. Acta* **1983**, *737*, 117−171.
(40) Jansson, M.; Thurmond, R. L.; Barry, J. A.; Brown, M. F. *J. Phys. Chem.* **1992**, *96*, 9532−9544.
(41) Petrache, H. I.; Tu, K.; Nagle, J. F. *Biophys. J.* **1999**, *76*, 2479−2487.
(42) Seelig, A.; Seelig, J. *Biochemistry* **1974**, *13*, 4839−4845.
(43) Thurmond, R. L.; Dodd, S. W.; Brown, M. F. *Biophys. J.* **1991**, *59*, 108−113.
(44) Douliez, J.-P.; Léonard, A.; Dufourc, E. J. *Biophys. J.* **1995**, *68*, 1727−1739.
(45) Smondyrev, A. M.; Berkowitz, M. L. *J. Chem. Phys.* **1999**, *110*, 3981−3985.

$$\langle A_C^{(n:0)} \rangle = \frac{2V_{CH_2}}{D_M} \left\langle \frac{1}{\cos \beta} \right\rangle \quad (7)$$

Here V_{CH_2} represents the volume of a methylene group, and $D_M = 2.54$ Å is the length of a virtual bond between carbons $i - 1$ and $i + 1$. As discussed previously,[35] the area factor $q \equiv \langle 1/\cos \beta \rangle$ can be approximated by

$$q \approx 3 - 3\langle \cos \beta \rangle + \langle \cos^2 \beta \rangle \quad (8)$$

which involves the first two moments of the orientational distribution function $f(\cos \beta)$, having odd and even parity, respectively. Both moments can be calculated from the measured order parameter S_{CD}. For each of the segments, the first moment $\langle \cos \beta \rangle$ is given by eq 3 above, while the second moment is given by[35]

$$\langle \cos^2 \beta \rangle = \frac{1 - 4S_{CD}}{3} \quad (9)$$

With the area factor q obtained from eq 8, we then calculate the average cross-sectional area per saturated acyl chain as

$$\langle A_C^{(n:0)} \rangle = q \frac{2V_{CH_2}}{D_M} \quad (10)$$

For comparison with the disaturated lipids, we also calculate the associated *volumetric thickness*, defined in relation with the saturated chain volume $V_C^{(n:0)}$ as

$$D_C^{(n:0)} \equiv \frac{V_C^{(n:0)}}{\langle A_C^{(n:0)} \rangle} \quad (11)$$

We emphasize that the structural parameters $D_C^{(n:0)}$ and $\langle A_C^{(n:0)} \rangle$ are based on measurements of the saturated *sn*-1 chain only. The average molecular area per chain $\langle A_C^{(n:0)} \rangle$, as well as the directly related volumetric thickness $D_C^{(n:0)}$, reflects the packing of the saturated (*n*:0) chain within the bilayer and accounts only for its contribution to the hydrocarbon region. We have argued that for disaturated lipid bilayers, the volumetric thickness $D_C^{(n:0)}$, defined as in eq 11, properly reflects the hydrophobic span of one monolayer.[35] However, even for symmetric disaturated lipids, $D_C^{(n:0)}$ is not necessarily equal to the average chain projection onto the bilayer normal, denoted by $L_C^{(n:0)}$, as discussed in refs 35, 41, and 46. The exact relationship between $D_C^{(n:0)}$ and $L_C^{(n:0)}$ depends on the inter-monolayer packing at the bilayer center and, in the case of mixed-chain polyunsaturated lipids, on possible length mismatch between the saturated *sn*-1 chain and the polyunsaturated *sn*-2 chain. Thus, for completeness, we report the results for the conventional chain projection, $L_C^{(n:0)}$, together with an additional quantity, denoted by $L_C^{*(n:0)}$.[35,41] The latter gives the chain extent between the second carbon ($i = 2$) and the ω-carbon ($i = n_C$), calculated as a sum of segmental projections, $\langle D_i \rangle$, along the bilayer normal,

$$L_C^{*(n:0)} \equiv \langle z^{(2)} \rangle - \langle z^{(n_C)} \rangle = \sum_{i=3,5,\ldots}^{n_C-1} \langle D_i \rangle \quad (12)$$

where $\langle z^{(i)} \rangle$ represents the average coordinate of carbon *i*. Note that the summation in eq 12 is performed over odd values of *i* only, from $i = 3$ to $n_C - 1$. The chain extent $L_C^{*(n:0)}$ is a well-defined structural parameter, but it does not account for chain contributions beyond the end carbons C_2 and C_{n_C}. To include these contributions, the conventional approach[30,35,41] defines the chain length (projection) $L_C^{(n:0)}$ as

$$L_C^{(n:0)} = \frac{1}{2} \sum_{i=2,3,\ldots}^{n_C-1} \langle D_i \rangle + \langle D_{n_C-1} \rangle \quad (13)$$

(46) Nagle, J. F. *Biophys. J.* **1993**, *64*, 1476−1481.

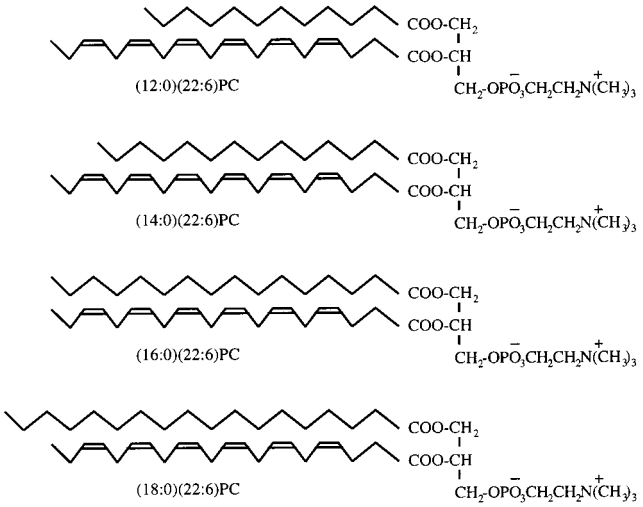

Figure 1. Schematic representation of (*n*:0-d_{2n-1})(22:6)PC chemical structures, for $n = 12$, 14, 16, and 18 carbons. As *n* is varied, the length mismatch between the (perdeuterated) saturated *sn*-1 acyl chain and the docosahexaenoic acid (DHA) *sn*-2 chain is altered. The ^{2}H-labeled saturated chain is used to monitor the average properties of the highly polyunsaturated bilayers in the fluid, liquid-crystalline (L_α) state. The chemical structures are drawn for heuristic purposes only, and do not show the energy minimized DHA conformations.

where the sum is now over all carbons from $i = 2$ to $i = n_C - 1$. The length $L_C^{(n:0)}$ is typically larger than L_C^* by 1−2 Å, but still less than the volumetric thickness $D_C^{(n:0)}$.[35]

Results

Deuterium NMR Spectroscopy of Docosahexaenoyl Phospholipids in the Liquid-Crystalline State. Solid-state ^{2}H NMR spectra were measured for the homologous series of mixed-chain lipids (*n*:0-d_{2n-1})(22:6)PC, with $n = 12$, 14, 16, and 18, at temperatures between −10 and 50 °C, as described below. Based on the chemical structures (see Figure 1), fully extended conformations (all-trans) of the *sn*-1 chains show a variable degree of length mismatch between the saturated *sn*-1 chain and the extended polyunsaturated *sn*-2 chain. The question is whether such a mismatch persists in fluid bilayers where, due to thermal disorder, the acyl chains assume a wide range of conformations. Consequently, one is interested in how the chain packing is affected by the intrinsic chain mismatch, and, ultimately, the effects on the bilayer properties. As we show next, such questions can be investigated in depth by ^{2}H NMR spectroscopy.

Representative solid-state ^{2}H NMR spectra acquired for the saturated *sn*-1 chain of the mixed-chain, polyunsaturated series are presented in Figure 2. The powder-type ^{2}H NMR spectra of the randomly oriented, multilamellar dispersions are shown at the left, and the de-Paked subspectra, corresponding to the $\theta = 0°$ orientation of the bilayer normal with respect to the magnetic field, are shown at the right. The quality of the spectra indicates a uniform spherical distribution of bilayer orientations, characteristic of homogeneous multilamellar lipid dispersions (so-called powder-type samples). In addition, the ^{2}H NMR spectra in Figure 2 indicate that the phospholipids undergo axially symmetric motions about the bilayer normal, with a distribution of quadrupolar splittings due to the various inequivalent methylene and methyl groups of the perdeuterated saturated acyl chains. Based on studies of specifically deuterated phospholipids in the L_α state,[42] it is known that the largest

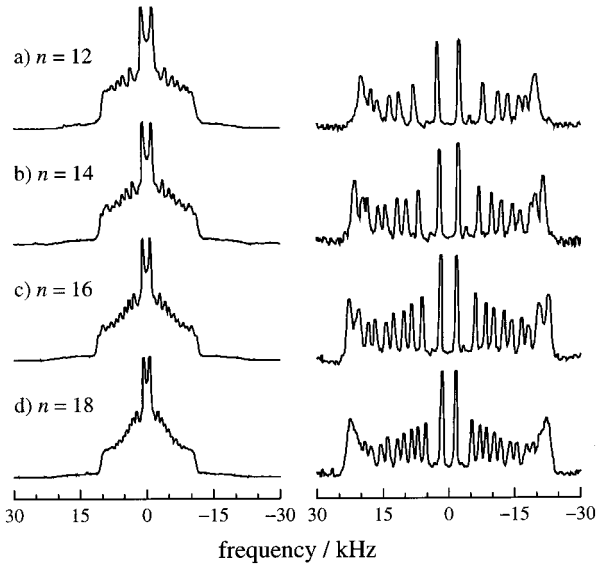

Figure 2. (a−d) Representative ^2H NMR spectra of the homologous series of mixed-chain, saturated−polyunsaturated phosphatidylcholines, (n:0-d_{2n-1})(22:6)PC, for n = 12, 14, 16, and 18 carbons. The phospholipids have a perdeuterated *sn*-1 acyl chain at the glycerol *sn*-1 position and a protiated DHA chain at the *sn*-2 position. Samples were fully hydrated (67 mM Na phosphate buffer, pH 7.0; 50 wt % H_2O) and were in the liquid-crystalline (L_α) state at 50 °C. Powder-type ^2H NMR spectra are shown at the left and the corresponding de-Paked ^2H NMR spectra at the right. As the *sn*-1 acyl length is increased, i.e., additional acyl mass is added to the hydrocarbon region, further quadrupolar splittings appear, in marked contrast to the behavior of disaturated phosphatidylcholines (see text).

quadrupolar splittings correspond to the acyl chain segments closest to the lipid−water interface (called the plateau region), followed by a progressive decrease along the chains toward the terminal methyl groups. We have assumed that the same trend holds for the mixed-chain, polyunsaturated lipid bilayers in the fluid, liquid-crystalline (L_α) state. The spectral assignments and the numerical quadrupolar splittings, $(\Delta\nu_Q)_{||}$, corresponding to the $\theta = 0°$ orientation, are summarized in Tables 1−4.

As shown previously by Salmon et al.,[30] the ^2H NMR spectra of multilamellar dispersions of (n:0-d_{2n-1})(22:6)PC lipids differ both qualitatively and quantitatively from those of disaturated phospholipids. Specifically, the former appear roughly triangular in shape (apart from the central methyl component), as opposed to the rectangular shape characteristic of disaturated phospholipids (not shown).[35] Moreover, an inspection of the line shapes in Figure 2 reveals an interesting behavior with increasing acyl chain length at fixed absolute temperature. Namely, the largest quadrupolar splittings *increase*, while the smaller splittings including the methyl group splitting *decrease* with increasing acyl chain length. The contrasting features of the ^2H NMR line shapes between the disaturated and the mixed-chain, polyunsaturated phosphatidylcholines are clearly visible in Figure 3, where we show the variation of the quadrupolar splittings ($\theta = 0°$) with acyl chain length for each series. For the disaturated series,[35] part a, the quadrupolar splittings $(\Delta\nu_Q)_{||}$ are roughly constant or increase slightly (positive slope), indicating equal or higher orientational order of the corresponding segments as the number of carbons (m) is increased. By contrast, for the polyunsaturated series, part b, the values of $(\Delta\nu_Q)_{||}$ for the *sn*-1 chain are seen to decrease (negative slope), indicating a reduction in the orientational order as the number of carbons (n) is increased. Note also that the number of resolved quadrupolar splittings is larger in the case of the polyunsaturated series and varies with the *sn*-1 acyl length. This is the result of increased acyl chain disorder (as compared to the disaturated series), which reduces the number of equivalent carbons with overlapping resonances (plateau region).

Order Parameter Profiles of Polyunsaturated Phospholipids. Further analysis of the ^2H NMR spectral data in terms of C—^2H bond order parameters allows for a more insightful comparison of polyunsaturated lipids among themselves and in relation to the corresponding disaturated lipid bilayers. Figure 4 shows the order parameters $|S_{CD}^{(i)}|$ as a function of carbon index (i) for the perdeuterated, saturated *sn*-1 chain adjacent to the *sn*-2 DHA chain for the homologous series of mixed-chain phosphatidylcholines in the liquid-crystalline (L_α) state. Each panel shows the data for a single lipid at temperatures ranging between −5 and 50 °C. The order profiles are typical for saturated acyl chains: there is an initial plateau region, corresponding to the acyl chain segments next to the glycerol and headgroup regions, followed by a monotonic decrease of the order parameters moving toward the chain ends closer to the bilayer center. As observed previously for disaturated lipids,[35] the global chain order decreases with increasing temperature, indicating increased thermal motion within the fluid lipid bilayers. A large effect of temperature is evident for the plateau region, which becomes more disordered as the temperature increases. In addition, one can identify a distinct subplateau region which seems to be the most sensitive to temperature variations. Especially for the longer (18:0-d_{35})(22:6)PC lipid, this corresponds to a change in curvature of the order profiles near the midchain region with increasing temperature.

Further comparison among the homologous phospholipids can be made at fixed absolute temperature. As shown previously,[35] and also seen in Figure 3, for the disaturated lipids the nonplateau order parameters depend only weakly on the acyl chain length, while those in the plateau region are higher for longer chains. Figure 5 shows that the mixed-chain, saturated−polyunsaturated lipids behave rather differently: at any given temperature, the nonplateau order parameters decrease as the acyl length increases, indicating increased disorder at the bilayer center as the saturated chain becomes longer (cf. also Figure 3). This suggests a broadening of the chain termination distribution along the bilayer normal, which could in principle be detectable by small-angle X-ray scattering.[47] A second observation, most noticeable at T = 50 °C, is that the order profiles for the different lipids tend to approach each other in the upper part of the acyl chain, indicating that the DHA chain imposes a stronger perturbation in this chain region. Similar results on the shape of the ^2H NMR order profile have been obtained by Holte et al.[25] using a steroyl (18:0) chain as a probe of the mixed-chain lipid systems. As we will show, further data reduction allows us to better resolve the differences between the two series. This will be discussed on the basis of a *universal chain packing profile*[35] that allows for a unified description of lipid bilayers.

Before discussing the chain packing profiles, however, let us first examine the global effect of the DHA chain on the bilayer structure. In this regard, there are two natural questions to address: (i) How is the lateral density (area per lipid) affected by DHA for the different *sn*-1 chain lengths? (ii) What is the variation of the bilayer thickness? We shall address these questions using a statistical model[35] to reduce the C−^2H bond order parameters to structural parameters, including average cross-sectional areas and average chain lengths. Specifically,

(47) Petrache, H. I.; Tristram-Nagle, S.; Nagle, J. F. *Chem. Phys. Lipids* **1998**, *95*, 83−94.

Table 1. De-Paked ^{2}H NMR Spectral Assignments and $(\Delta\nu_Q)_{||}$ Splittings for (12:0-d_{23})(22:6)PC in the Liquid-Crystalline (L_α) Phase

peak	carbon *i*	$(\Delta\nu_Q)_{||}$ /kHz[a]								
		−9 °C	−5 °C	0 °C	5 °C	10 °C	15 °C	20 °C	30 °C	50 °C
A	2−6	64.1	57.6	55.9	53.1	51.5	49.9	47.8	44.7	39.6
B	7	64.1	53.3	51.5	48.8	46.8	45.0	43.3	39.5	34.7
C	8	58.6	50.6	48.2	45.4	43.5	41.7	40.2	36.5	31.7
D	9	50.9	43.4	41.0	38.4	36.7	35.1	33.4	30.2	25.9
E	10	44.1	37.3	35.4	32.9	31.2	29.7	28.2	25.5	21.5
F	11	33.2	26.9	25.5	23.6	22.3	21.0	20.0	17.8	15.0
G	12	11.1	9.5	8.6	8.0	7.5	6.8	6.6	5.7	4.6

[a] Quadrupolar splitting corresponding to $\theta = 0°$ orientation of bilayer normal with respect to magnetic field.

Table 2. De-Paked ^{2}H NMR Spectral Assignments and $(\Delta\nu_Q)_{||}$ Splittings for (14:0-d_{27})(22:6)PC in the Liquid-Crystalline (L_α) Phase

peak	carbon *i*	$(\Delta\nu_Q)_{||}$ /kHz[a]								
		0 °C	15 °C	22.5 °C	25 °C	30 °C	35 °C	40 °C	45 °C	50 °C
A	2−4	59.7	53.6	51.4	50.4	48.5	47.6	46.4	45.0	43.5
B	5−7	54.8	49.4	47.6	46.6	44.5	44.1	42.6	41.3	39.3
C	8	54.8	47.8	46.3	44.4	42.3	41.4	39.6	37.8	36.3
D	9	48.6	41.9	39.8	38.5	36.8	35.6	34.3	32.8	31.5
E	10	44.4	37.7	35.6	34.6	32.8	31.6	30.7	29.2	27.5
F	11	37.2	31.4	29.0	28.2	27.0	25.8	24.8	23.6	22.3
G	12	31.7	26.2	24.5	23.3	22.2	21.1	20.3	19.4	18.1
H	13	23.0	18.7	17.0	16.5	15.7	14.7	14.3	13.4	12.8
I	14	7.4	6.0	5.4	5.4	4.9	4.5	4.3	4.1	3.8

[a] Quadrupolar splitting corresponding to $\theta = 0°$ bilayer orientation.

Table 3. De-Paked ^{2}H NMR Spectral Assignments and $(\Delta\nu_Q)_{||}$ Splittings for (16:0-d_{31})(22:6)PC in the Liquid-Crystalline (L_α) Phase

peak	carbon *i*	$(\Delta\nu_Q)_{||}$ /kHz[a]						
		−5 °C	0 °C	5 °C	10 °C	15 °C	30 °C	50 °C
A	2−5	67.1	61.5	58.7	57.7	55.8	51.1	45.2
B	6−7	67.1	61.5	58.7	54.5	52.2	46.2	41.9
C	8	67.1	61.5	58.7	54.5	52.2	46.2	39.4
D	9	61.8	54.8	52.2	49.3	47.1	40.9	35.2
E	10	58.8	53.0	48.4	45.8	43.8	37.7	31.8
F	11	52.2	44.9	42.3	40.0	37.9	32.2	26.5
G	12	47.4	40.9	37.7	35.6	33.7	28.2	23.0
H	13	39.8	34.0	31.5	29.5	27.8	22.9	18.5
I	14	33.7	28.6	26.5	24.6	23.1	18.9	15.1
J	15	24.7	21.1	19.3	18.0	16.8	13.7	10.8
K	16	7.8	6.7	6.1	5.6	5.2	4.1	3.0

[a] Quadrupolar splitting corresponding to $\theta = 0°$ bilayer orientation.

Table 4. De-Paked ^{2}H NMR Spectral Assignments and $(\Delta\nu_Q)_{||}$ Splittings for (18:0-d_{35})(22:6)PC in the Liquid-Crystalline (L_α) Phase

peak	carbon *i*	$(\Delta\nu_Q)_{||}$ /kHz[a]							
		−5 °C	0 °C	5 °C	10 °C	15 °C	20 °C	30 °C	50 °C
A	2−7	65.2	62.4	59.1	56.7	54.7	53.4	51.2	46.4
B	8	65.2	62.4	59.1	56.7	54.7	53.4	51.2	42.6
C	9	65.2	57.8	53.4	51.5	49.5	47.5	43.9	37.5
D	10	59.4	55.3	51.2	49.0	45.5	44.3	40.8	34.5
E	11	54.5	49.8	45.9	43.5	40.5	39.0	35.6	29.8
F	12	50.9	45.8	41.8	39.8	37.1	35.4	32.0	26.3
G	13	44.8	40.2	36.5	34.5	32.1	30.2	26.9	22.1
H	14	41.2	36.4	32.4	30.9	28.3	26.8	23.6	18.7
I	15	34.7	30.7	27.3	25.9	23.6	22.2	19.7	15.7
J	16	29.7	26.0	23.2	21.8	19.9	18.7	16.4	12.9
K	17	22.6	19.6	17.4	16.3	14.9	14.1	12.3	9.8
L	18	7.3	6.3	5.4	5.2	4.6	4.3	3.7	2.8

[a] Quadrupolar splitting corresponding to $\theta = 0°$ bilayer orientation.

the analysis of the order parameters is done in terms of acyl chain orientational distributions, within the framework of a mean-torque model[35] previously used for disaturated lipid ^{2}H NMR data.

Structural Parameters of Mixed-Chain Polyunsaturated Phosphatidylcholines. For each of the lipids in the (*n*:0-d_{2n-1})-(22:6)PC series, we have used the ^{2}H NMR order parameters of the perdeuterated, saturated *sn*-1 chain (see Tables 1−4 for the measured quadrupolar splittings) to calculate its molecular cross-sectional area $\langle A_C^{(n:0)}\rangle$ and molecular volumetric thickness $D_C^{(n:0)}$ as a function of temperature and acyl chain length *n* (see Methods). In analogy with the concept of partial molar quantities, one can also introduce the partial molecular volumes of the saturated and polyunsaturated acyl components as follows, where the bilayer is treated as a continuum medium. The total differential of the hydrocarbon chain volume is

$$dV_C = \left(\frac{\partial V_C}{\partial n_{n:0}}\right)_{T,P} dn_{n:0} + \left(\frac{\partial V_C}{\partial n_{22:6}}\right)_{T,P} dn_{22:6} \quad (14)$$

$$\equiv V_C^{(n:0)}\, dn_{n:0} + V_C^{(22:6)}\, dn_{22:6} \quad (15)$$

Here $n_{n:0}$ denotes the number of saturated (*n*:0) chains and $n_{22:6}$ the number of polyunsaturated (22:6) chains, where $V_C^{(n:0)}$ and $V_C^{(22:6)}$ are the associated partial molecular volumes. Integration of eq 15 holding the component ratios constant leads to the following sum rule for the mixed-chain bilayer:

$$V_C = V_C^{(n:0)} n_{n:0} + V_C^{(22:6)} n_{22:6} \quad (16)$$

where $n_{n:0} = n_{22:6}$. The volumetric thickness of the bilayer can then be written in terms of the partial volumes and the total interfacial area, $\langle A\rangle = \langle A_C^{(n:0)}\rangle + \langle A_C^{(22:6)}\rangle$, as

$$D_C \equiv \frac{V_C}{\langle A\rangle} = \frac{V_C^{(n:0)} + V_C^{(22:6)}}{\langle A_C^{(n:0)}\rangle + \langle A_C^{(22:6)}\rangle} \quad (17)$$

Note that this definition for the hydrocarbon thickness (per monolayer) D_C is consistent with the bilayer structure determination from small-angle X-ray scattering data.[35,47]

Using the ^{2}H NMR data for the saturated *sn*-1 chain, we can calculate the partial cross-sectional area $\langle A_C^{(n:0)}\rangle$ of this chain,

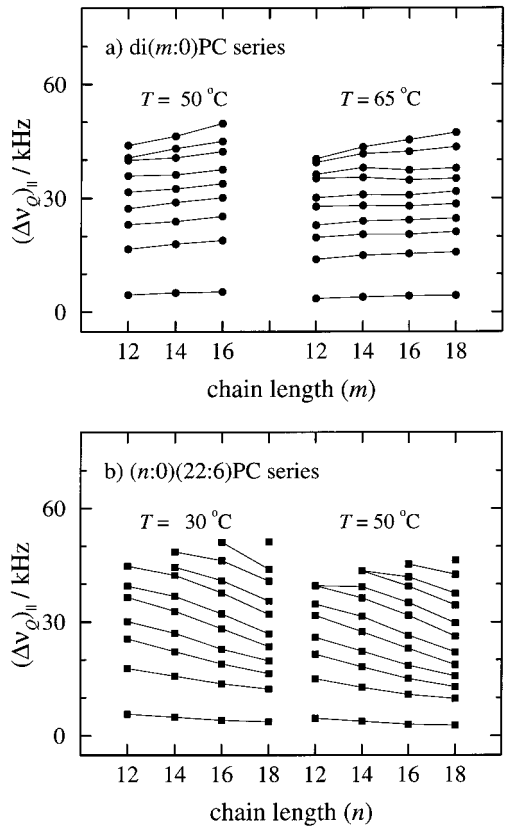

Figure 3. Dependence of ^2H NMR quadrupolar splittings ($\theta = 0°$) on perdeuterated *sn*-1 acyl chain length n_C ($\equiv m$ or n) for (a) the disaturated phosphatidylcholine series, di(m:0-d_{2m-1})PC, and (b) the mixed-chain (n:0-d_{2n-1})(22:6)PC series in the L_α state. Data in part a are from ref 35. Note that for the disaturated PC series, part a, the quadrupolar splittings $(\Delta\nu_Q)_\parallel$ remain approximately constant or increase slightly with increasing *sn*-1 acyl chain length at the same absolute temperature. The new splittings are near the largest (plateau) values and increase with the acyl length. By contrast, for the mixed-chain polyunsaturated series, part b, the quadrupolar splittings decrease with increasing *sn*-1 acyl carbons at the same absolute temperature, so that the new splittings at larger values are accompanied by additional intermediate splittings. Consequently, the packing of the (saturated) *sn*-1 acyl chains must differ substantially in the two cases.

as explained in Methods. One needs additional information, viz. $\langle A_C^{(22:6)}\rangle$, to determine the total lipid cross-sectional area $\langle A\rangle$ and the hydrocarbon half-thickness D_C, as we show later. Note that for the disaturated series, because of the chain symmetry, one has $V_C = 2V_C^{(n:0)}$ and $\langle A\rangle = 2\langle A_C^{(n:0)}\rangle$, and consequently $D_C = D_C^{(n:0)}$. The situation is more complicated for the mixed-chain bilayers, where the hydrocarbon thickness per monolayer, D_C, may differ from $D_C^{(n:0)}$, depending on the structural parameters of the *sn*-2 chain, viz. $V_C^{(22:6)}$ and $\langle A_C^{(22:6)}\rangle$, as indicated by eq 17. However, it is still useful to consider the (partial) volumetric thickness due to the *sn*-1 chain, $D_C^{(n:0)}$, as defined by eq 11, for comparison with previous results for the disaturated series.[35] The values of $D_C^{(n:0)}$ and $\langle A_C^{(n:0)}\rangle$ for the mixed-chain polyunsaturated bilayers, obtained using eq 11 and eq 10 respectively, are shown in Figure 6. The saturated chain volumes $V_C^{(n:0)}$ were calculated using the temperature dependence given by $V_{CH_2} \approx V^0_{CH_2} + \alpha_{CH_2}(T - 273.15\ \mathrm{K})$, with empirical parameters $V^0_{CH_2} = 26.5$ Å^3 and $\alpha_{CH_2} = 0.0325$ Å^3 K^{-1}.[35] In addition, it was assumed that the terminal methyl volume V_{CH_3} is roughly twice the methylene volume V_{CH_2}.[48−50] The area results in Figure 6 are plotted as $2\langle A_C^{(n:0)}\rangle$ to enable comparison

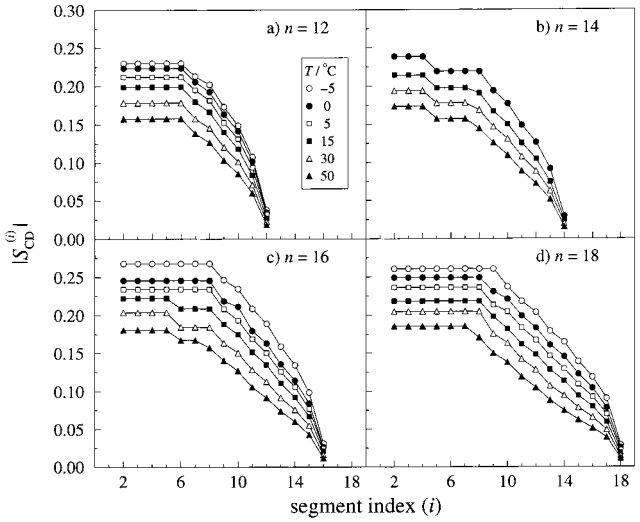

Figure 4. Order parameters, $|S_{CD}^{(i)}|$, of acyl chain C$-^2$H bonds as a function of segment index i, for the (n:0-d_{2n-1})(22:6)PC series in the liquid-crystalline (L_α) state. Each panel shows the data for one member of the series at various temperatures. Note that the overall order decreases with increasing temperature, and that a larger effect is observed on the initial carbon segments (plateau region). Consequently, the order profiles do not scale uniformly with temperature, implying a differential thermal expansion along the acyl chains.

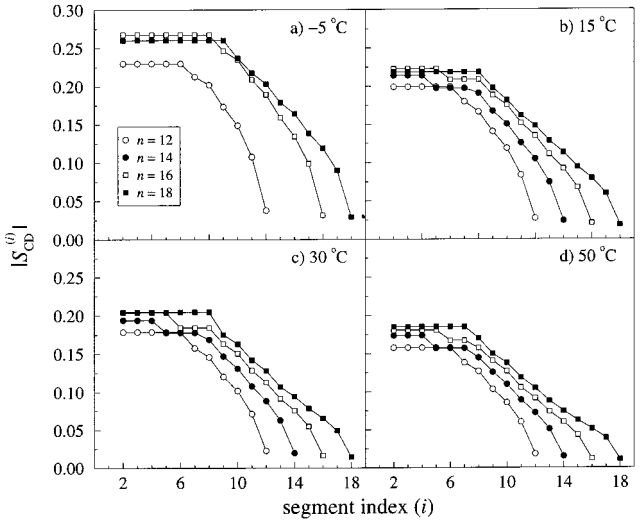

Figure 5. Same data as in Figure 4, but now each panel compares the different lipids at the same absolute temperature. As the number of carbons in the *sn*-1 acyl chain increases, the order parameters of the initial segments increase, while those of the end segments decrease, causing a noticeable change of shape of the order profile.

with previous results for disaturated lipids, where the total area per molecule $\langle A\rangle = 2\langle A_C^{(n:0)}\rangle$ corresponds to both acyl chains. A summary of the structural results is provided in Table 5.

From part a of Figure 6 we note that the partial volumetric thickness $D_C^{(n:0)}$ decreases with temperature, as for the disaturated lipids, while at fixed absolute temperature, $D_C^{(n:0)}$ increases with increasing number of carbons in the acyl chain (larger n). Moreover, the overall variation with temperature is similar for the two homologous series, with the polyunsaturated

(48) Nagle, J. F.; Wilkinson, D. A. *Biophys. J.* **1978**, *23*, 159−175.
(49) Petrache, H. I.; Feller, S. E.; Nagle, J. F. *Biophys. J.* **1997**, *72*, 2237−2242.
(50) Armen, R. S.; Uitto, O. D.; Feller, S. E. *Biophys. J.* **1998**, *75*, 734−744.

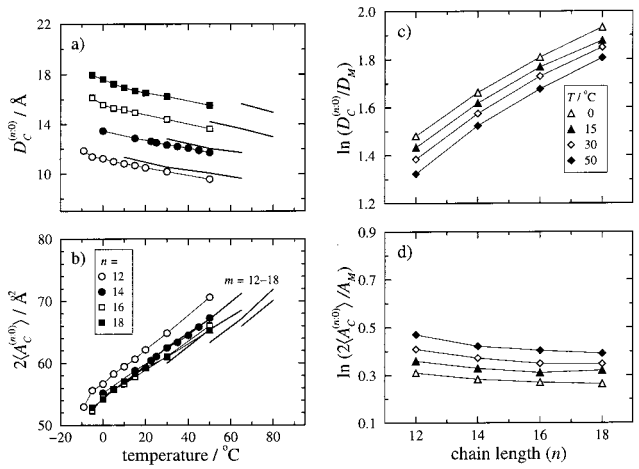

Figure 6. Structural parameters of the saturated *sn*-1 chain, as a function of temperature (a,b) and acyl chain length (c,d). Parts a and b show results for the partial volumetric thickness, $D_C^{(n:0)}$, and twice the partial area per saturated chain, $2\langle A_C^{(n:0)}\rangle$, respectively, for the mixed-chain, (*n*:0-d_{2n-1})(22:6)PC, lipids. The thick lines show corresponding results for the disaturated series, di(*m*:0-d_{2m-1})PC, taken from ref 35. At a given absolute temperature, acyl polyunsaturation at the *sn*-2 position generates a smaller hydrocarbon thickness and a larger cross-sectional area. Parts c and d show semilogarithmic plots of the relative variation of $D_C^{(n:0)}$ and $2\langle A_C^{(n:0)}\rangle$ for the mixed-chain polyunsaturated series. The reference values D_M and A_M represent the maximum segmental projection onto the bilayer normal and the corresponding minimum area ($A_M \equiv 4V_{CH_2}/D_M$), respectively. The effect of increasing the saturated acyl length *n* (mass added to the system) is reflected more on the partial volumetric thickness, $D_C^{(n:0)}$, than on the cross-sectional area, $\langle A_C^{(n:0)}\rangle$.

curves being slightly shifted to lower $D_C^{(n:0)}$ values (by roughly 0.5 Å). Alternatively, the two sets of curves can be made to overlap by a relative shift along the temperature axis of about 15−20 °C. This shows that at the same absolute temperature, the saturated *sn*-1 chains of the DHA lipids are more disordered than for the corresponding disaturated series, which results in smaller values of $D_C^{(n:0)}$ and larger cross-sectional areas $\langle A_C^{(n:0)}\rangle$. One should also note that the area differences among the polyunsaturated lipids are significantly smaller than the spread of cross-sectional areas of their disaturated counterparts, as shown in part b of Figure 6. With the exception of the (12:0)-(22:6)PC bilayer, the polyunsaturated lipids have roughly the same area per saturated chain, especially in the temperature range below 30 °C. This important result suggests that the short (12:0) chain is a special case, namely there is a qualitative difference between the way the DHA chain packs with the short (12:0) *sn*-1 chain and with the other longer saturated chains. This aspect will be further considered in the Discussion section.

Let us next turn to the acyl chain length dependence of the structural parameters for the mixed-chain, polyunsaturated bilayers. The relative variations of $D_C^{(n:0)}$ and $\langle A_C^{(n:0)}\rangle$ with the saturated acyl chain length *n* are shown in parts c and d of Figure 6. The advantage of plotting the relative (dimensionless) variations in semilogarithmic fashion is that the effects of the chain length on the thickness and area per chain can now be directly compared. It can be seen that as mass is added to the saturated *sn*-1 chain, the thickness $D_C^{(n:0)}$ increases, while the area per chain $\langle A_C^{(n:0)}\rangle$ undergoes a slight contraction. Clearly, there is a more pronounced effect of the additional acyl mass on the bilayer thickness, rather than on the area. Consequently, for the polyunsaturated series, as found previously for the disaturated series,[35] the major influence on the area per lipid comes from the polar headgroups rather than the acyl length. The fact that the area per lipid decreases with increasing acyl chain length might appear counterintuitive at first, considering the repulsion generated by chain confinement. The explanation, however, resides in the fact that longer chains (more mass added) have increased van der Waals attraction that overcomes repulsive entropic effects. In effect, the longer chains keep the headgroups closer together on average, in agreement with the higher melting temperatures.[35]

Material Properties of DHA Lipids Revealed by the Saturated Chain Behavior. To better quantify the variation of the structural parameters with both the thermodynamic variable *T* and the carbon number *n*, let us consider the following total differential:[35]

$$\frac{1}{V}\mathrm{d}V = \frac{1}{V}\left(\frac{\partial V}{\partial T}\right)_{n,P}\mathrm{d}T + \frac{1}{V}\left(\frac{\partial V}{\partial n}\right)_{T,P}\mathrm{d}n \equiv \alpha\,\mathrm{d}T + \nu\,\mathrm{d}n \tag{18}$$

The above total differential defines the total volumetric expansion coefficients α and ν under conditions of constant bulk pressure *P*. The coefficient α represents the thermal expansion, while ν describes the relative volume change due to additional carbons, and reduces to $\nu = 1/n$. Using the relationship $V_C^{(n:0)} = D_C^{(n:0)}\langle A_C^{(n:0)}\rangle$ (and suppressing the superscript (*n*:0) for clarity), we can write

$$\frac{\mathrm{d}V_C}{V_C} = \mathrm{d}\ln V_C = \frac{\mathrm{d}D_C}{D_C} + \frac{\mathrm{d}\langle A_C\rangle}{\langle A_C\rangle} = \mathrm{d}\ln D_C + \mathrm{d}\ln\langle A_C\rangle \tag{19}$$

This expression allows for a decomposition of the two bulk coefficients α and ν into contributions from the relative thickness variation (parallel component) and the relative area variation (perpendicular component):

$$\alpha \equiv \left(\frac{\partial \ln V_C}{\partial T}\right)_{n,P} = \left(\frac{\partial \ln D_C}{\partial T}\right)_{n,P} + \left(\frac{\partial \ln\langle A_C\rangle}{\partial T}\right)_{n,P} \equiv \alpha_{\parallel} + \alpha_{\perp} \tag{20}$$

and

$$\nu \equiv \left(\frac{\partial \ln V_C}{\partial n}\right)_{T,P} = \left(\frac{\partial \ln D_C}{\partial n}\right)_{T,P} + \left(\frac{\partial \ln\langle A_C\rangle}{\partial n}\right)_{T,P} \equiv \nu_{\parallel} + \nu_{\perp} \tag{21}$$

The above expansion coefficients, calculated by interpolation of the structural parameters from Figure 6, are given in Table 5. Note that the isobaric thermal expansion of the saturated *sn*-1 chain, quantified by $\alpha_{\parallel}$ and $\alpha_{\perp}$, is similar for both the disaturated and the mixed-chain polyunsaturated series. The thickness $D_C^{(n:0)}$ decreases with temperature by a fractional change $\alpha_{\parallel}$ on the order of -2×10^{-3} to -4×10^{-3} K^{-1}, while the partial cross-sectional area $\langle A_C^{(n:0)}\rangle$ increases with $\alpha_{\perp}$ between 3×10^{-3} and 5×10^{-3} K^{-1}. The reason the thermal expansion coefficients for the disaturated and polyunsaturated series are similar is evident from Figure 6. While the magnitude of the structural parameters varies between the two series, the thermal variation is the same. In particular, a relative temperature shift of 15−20 °C would make the two families of curves overlap.

Discussion

Effect of Docosahexaenoyl Acyl Chains on Bilayer Properties. Polyunsaturated lipids are found as constituents of cellular

Table 5. Summary of Structural Results for Saturated *sn*-1 Chain of (*n*:0)(22:6)PC Lipids in the Liquid-Crystalline (L_α) State

n	*T*/°C	S_p[a]	$D_C^{(n:0)}$/Å[b]	$\langle A_C^{(n:0)}\rangle$/Å^2 [c]	$\alpha_{\|}/10^{-3}$K^{-1} [d]	$\alpha_\perp/10^{-3}$K^{-1} [e]	$\nu_{\|}/10^{-2}$ [f]	$\nu_\perp/10^{-2}$ [g]	$L_C^{*(n:0)}$/Å[h]	$L_C^{(n:0)}$/Å[i]
12	0	0.223	11.2	28.3	−3.1	4.3	11.3	−3.0	8.8	10.4
	30	0.179	10.2	32.4	−3.2	4.4	13.5	−5.2	7.9	9.3
	50	0.158	9.6	35.3	−3.4	4.6	13.4	−5.0	7.5	8.8
14	0	0.238	13.5	27.6	−3.6	4.8	9.3	−2.1	10.6	12.2
	30	0.194	12.3	31.2	−2.6	3.8	10.8	−3.7	9.6	10.9
	50	0.174	11.7	33.6	−2.7	3.9	10.7	−3.5	9.0	10.2
16	0	0.246	15.6	27.2	−3.9	5.1	7.9	−1.6	12.5	14.1
	30	0.204	14.4	30.6	−2.6	3.8	9.0	−2.7	11.2	12.5
	50	0.181	13.6	33.0	−2.7	3.9	8.9	−2.6	10.5	11.6
18	0	0.249	17.6	27.1	−4.1	5.4	6.8	−1.3	14.3	15.8
	30	0.205	16.2	30.5	−2.1	3.3	7.7	−2.2	12.6	13.9
	50	0.185	15.5	32.6	−1.9	3.1	7.6	−2.1	11.9	13.0

[a] Plateau order parameter values used to calculate the area factor *q* (eq 8). [b] Volumetric thickness (eq 11). [c] Cross-sectional area (eq 10). [d] Thermal expansion coefficient along the bilayer normal (eq 20). [e] Thermal expansion coefficient in the membrane plane (eq 20). [f] Volumetric expansion coefficient along the bilayer normal due to additional carbons (eq 21). [g] Volumetric expansion coefficient in the membrane plane due to additional carbons (eq 21). [h] Average chain projection calculated using eq 12. [i] Average chain projection calculated using eq 13.

membranes, and thus knowledge of their structural properties is needed to understand their roles in biological membrane function.[12,13] One hypothesis regarding the role of polyunsaturated lipids in biological functions (such as vision) is based on the distinct physical properties of lipid bilayers conferred by the presence of the polyunsaturated chain.[14,23,53] For instance, a native-like lipid environment involving the presence of phospholipid DHA chains is sufficient, although not necessary for native-like visual function of rhodopsin in the membrane.[53−56] Rather, biophysical properties of the membrane bilayer appear to be involved in the meta I−meta II transition of rhodopsin, the signal transducing event of visual excitation. As a rule, the properties of lipid bilayers are governed by a balance of forces acting on both the headgroup (hydrophilic) and hydrocarbon (hydrophobic) regions. We have observed that introduction of a polyunsaturated DHA chain at the *sn*-2 position increases the cross-sectional area per lipid headgroup in liquid-crystalline bilayers.[30] Consequently, the force balance is shifted according to the modified acyl chain interactions, inducing a change in the curvature stress involving the aqueous interface. This aspect has been addressed in the literature with regard to the "spontaneous curvature" induced by the effective lipid shape.[23,57,58]

The specific structural and dynamical properties of polyunsaturated lipids are best revealed by comparison with saturated bilayers.[25,30] In this regard, a deeper understanding can be acquired by comparison of the members of a homologous series, rather than individual lipids.[22,25,34] Therefore, we have analyzed the properties of the polyunsaturated (*n*:0)(22:6)PC bilayers in relation to the disaturated di(*m*:0)PC series.[34] Based on chemical structures (Figure 1), the mixed-chain (*n*:0)(22:6)PC series is characterized by a systematic variation of the acyl chain mismatch as the *sn*-1 acyl length is varied. While this intrinsic mismatch might not be fully preserved in bilayers formed at finite temperatures, it is expected to influence the bilayer properties.

Length Mismatch and Area Differences between the Saturated and Polyunsaturated Acyl Chains in Fluid Bilayers. Let us first note that the polyunsaturated DHA chain has a larger molecular volume than any of the saturated chains considered in this study. At 30 °C, for example, one estimates a DHA molecular volume of about 526.4 Å^3, using $V_{CH_2} =$ 27.475 Å^3 (see above) and assuming a ratio V_{CH_2}/V_{CH} of $\approx$1.31.[59] With $V_C^{(22:6)} =$ 526.4 Å^3, the ratio between the *sn*-1 and the *sn*-2 chain volumes in the mixed-chain, saturated−polyunsaturated series is found to vary from 0.63 for $n = 12$ to 0.94 for $n = 18$. Given that the DHA chain has a large molecular volume, the question is whether the DHA chain contributes to enlarging the cross-sectional area, increasing the bilayer thickness, or both. There are only a few reported measurements on the interfacial area of DHA-containing lipid bilayers. For fully hydrated (18:0)(22:6)PC at 30 °C, Koenig et al.[51] give a value of $\langle A\rangle = 69.2$ Å^2 from a combined ^{2}H NMR and X-ray analysis. Subtracting our results for the *sn*-1 partial area $\langle A_C^{(18:0)}\rangle = 30.5$ Å^2 (cf. Table 5), we obtain $\langle A_C^{(22:6)}\rangle = 38.7$ Å^2 for the DHA chain. This suggests that the DHA molecular cross-sectional area is larger than that of the adjacent (18:0) chain by 8−9 Å^2. We can therefore conclude that the larger cross-sectional area for the mixed-chain (*n*:0)(22:6)PC bilayer is due to both chains: not only is the *sn*-1 chain more disordered, but also the DHA chain is larger.[25,52] Note that this decomposition into partial areas associated with each chain does not make any particular assumption about the shape of the two chains. The results for the partial areas give a ratio $\langle A_C^{(18:0)}\rangle/\langle A_C^{(22:6)}\rangle \approx 0.79$. Since this is not equal to the volumetric ratio calculated above, it implies that a mismatch of chain length projections along the bilayer normal is also present. To explore this possibility, we consider the DHA volumetric thickness defined as $D_C^{(22:6)} \equiv V_C^{(22:6)}/\langle A_C^{(22:6)}\rangle$. With the volume and area values from above, we obtain $D_C^{(22:6)} \approx$13.6 Å, with an error estimate of ±0.3 Å. Compared to $D_C^{(18:0)} =$ 16.2 Å for the saturated (18:0) chain (Table 5), it shows that the DHA volumetric thickness, $D_C^{(22:6)}$, is lower by 2−3 Å. As mentioned above, the hydrophobic thickness (per monolayer) D_C is calculated from eq 17 using the lipid total hydrocarbon volume and total cross-sectional area. For (18:0)(22:6)PC at 30 °C we obtain $D_C =$ 14.8 Å, which is an intermediate value between $D_C^{(22:6)} =$ 13.6 Å and $D_C^{(18:0)} =$ 16.2 Å, as expected from eq 17. The relationship between D_C and the single-chain volumetric thicknesses, $D_C^{(n:0)}$ and $D_C^{(22:6)}$,

(51) Koenig, B. W.; Strey, H. H.; Gawrisch, K. *Biophys. J.* **1997**, *73*, 1954−1966.
(52) Applegate, K. R.; Glomset, J. A. *J. Lipid Res.* **1986**, *27*, 658−680.
(53) Wiedmann, T. S.; Pates, R. D.; Beach, J. M.; Salmon, A.; Brown, M. F. *Biochemistry* **1988**, *29*, 6469−6474.
(54) Brown, M. F.; Gibson, N. J. In *Essential Fatty Acids and Eicosanoids*; Sinclair, A., Gibson, R., Eds.; American Oil Chemist's Society Press: Champaign, IL, 1992; pp 134−138.
(55) Gibson, N. J.; Brown, M. F. *Biochemistry* **1993**, *32*, 2438−2454.
(56) Botelho, A. V.; Gibson, N. J.; Wang, Y.; Thurmond, R. L.; Brown, M. F. *Biophys. J.* **2001**, *80*, 2466.
(57) Gruner, S. M.; Shyamsunder, E. *Ann. N. Y. Acad. Sci.* **1991**, *625*, 685−697.
(58) Gawrisch, K.; Holte, L. L. *Chem. Phys. Lipids* **1996**, *81*, 105−116.
(59) Marsh, D. *CRC Handbook of Lipid Bilayers*; CRC Press: Boca Raton, FL, 1992.

can be better seen by rewriting eq 17 as

$$D_C = \frac{\langle A_C^{(n:0)} \rangle}{\langle A \rangle} D_C^{(n:0)} + \frac{\langle A_C^{(22:6)} \rangle}{\langle A \rangle} D_C^{(22:6)} \qquad (22)$$

This expression shows that the hydrophobic thickness, D_C, can be regarded as an average of single-chain volumetric thicknesses, weighted by the partial areas. In this sense, the single-chain volumetric thicknesses play the role of partial quantities with respect to the hydrocarbon thickness D_C.

Note that the partial thicknesses $D_C^{(n:0)}$ and $D_C^{(22:6)}$ may, in general, differ from the geometric chain length projections, denoted by $L_C^{(n:0)}$ and $L_C^{(22:6)}$, calculated as a sum over segmental projections (see Methods). As discussed in detail elsewhere,[35,41,46] due to the highly disordered acyl chains in the fluid state, the hydrophobic thickness D_C depends on the chain packing at the bilayer center (inter-monolayer packing) and differs from the average chain length $L_C^{(n:0)}$. This is true for both the like-chain, disaturated bilayers and for the mixed-chain, saturated−polyunsaturated bilayers. For example, as shown in Table 5, for the (18:0)(22:6)PC at 30 °C, we estimate for the saturated chain length a value of $L_C^{(18:0)} = 13.9$ Å, to be compared to $D_C^{(18:0)} = 16.2$ Å. A discussion of chain length mismatch would more naturally involve the two chain length projections $L_C^{(n:0)}$ and $L_C^{(22:6)}$, but the latter cannot be estimated from the current data. As an alternative, we have considered the partial volumetric thicknesses $D_C^{(n:0)}$ and $D_C^{(22:6)}$. These can both be determined and conveniently used to characterize the structure of mixed-chain polyunsaturated bilayers in comparison with the disaturated series and X-ray data.[35,47] In particular, for like-chain disaturated bilayers, the volumetric thicknesses of the two acyl chains are expected to be the same. This is no longer true for the mixed-chain lipids, as we discuss next.

To discuss how the chain mismatch varies with the number of *sn*-1 carbons (n), let us assume a constant DHA area at fixed temperature. This is reasonable since only a slight area contraction is expected as hydrocarbon mass is added in the hydrocarbon region (see above). This means that the value of $\langle A_C^{(22:6)} \rangle = 38.7$ Å^2 obtained for $n = 18$ is an underestimate for shorter chains. However, the underestimate is more likely to be on the order of 1 Å^2, even for the extreme case of $n = 12$ studied here. Constant $\langle A_C^{(22:6)} \rangle$ would then imply constant volumetric thickness $D_C^{(22:6)}$ across the series at a given absolute temperature. In Figure 7, the estimated $D_C^{(22:6)}$ value (assumed constant) for the (n:0)(22:6)PC series at 30 °C is compared with the saturated chain volumetric thickness $D_C^{(n:0)}$ and with the hydrophobic thickness per monolayer, D_C. The results suggest that the volumetric thickness mismatch between the *sn*-1 and the *sn*-2 chains is minimal for $n = 14$ and $n = 16$, and crosses over in between. Interestingly, the value of $D_C = 13.0$ Å for (14:0)(22:6)PC from Figure 7 is practically the same as the hydrocarbon thickness per monolayer for di(14:0)PC, obtained previously.[35]

At this juncture, the DHA chain conformations deserve some attention. We have found that at 30 °C, the DHA chain occupies a partial cross-sectional area that is larger by 8−9 Å^2 than the saturated chain area. How can one interpret this result in terms of DHA conformations? Unfortunately, the specific DHA conformations and acyl packing are harder to determine. Typically, detailed molecular dynamics simulations are needed to explore the complex configurational space generated by the polyallylic sequence of alternating cis double bonds separated by single methylene carbons.[60] In principle, the DHA conformations are dominated by two preferred configurations, denoted as angle-iron and helical. These conformations have been considered by Applegate and Glomset[52] in the context of energy-minimized (optimal) DHA chain packing. Only recently have renewed computational efforts been directed toward polyunsaturated phospholipids in the fluid state, in an attempt to determine the accessible DHA states at biologically relevant temperatures. Huber et al.[60] have shown that, while DHA has a tendency to adopt extended conformations (helical, angle-iron) involving triene sequences, a large number of other disordered conformations are significantly populated, including back bending (chain upturns), all of which loosen the chain packing and increase the lipid cross-sectional area. Even at low temperatures, Applegate and Glomset[52] found a wide range of DHA cross-sectional areas, between 25.8 and 32.9 Å^2, depending on the chain arrangement. Angle-iron DHA shapes tended to give lower values of the cross-sectional area than helical conformations. In addition, somewhat lower cross-sectional areas were found for DHA chains packed together with saturated chains in all-trans configurations,[52] with an optimum DHA area between 24.3 and 27.0 Å^2. Noting that optimal packing of all-trans saturated chains occurs at roughly 20 Å^2 per chain,[52,61] this finding suggests that, in its energy-minimized state, the DHA chain occupies a lateral area which is larger by about 4−7 Å^2. It is therefore plausible that, as the temperature is increased, the area difference increases to 8−9 Å^2 at 30 °C, as we find in this study.

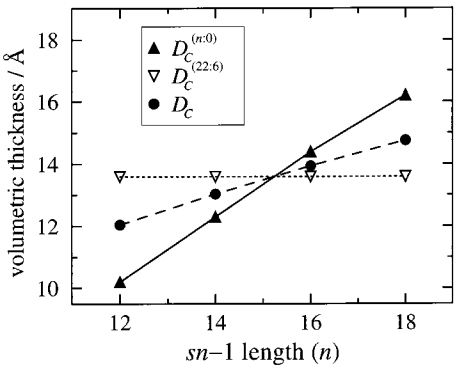

Figure 7. Volumetric thickness results for the (n:0-d_{2n-1})(22:6)PC series at 30 °C, showing the partial volumetric thicknesses $D_C^{(n:0)}$ and $D_C^{(22:6)}$ due to the individual chains, and the total hydrocarbon half-thickness (i.e., thickness per monolayer) D_C (eq 17). The asymmetric distribution of mass along the lipid long axis generates an acyl length mismatch between the saturated *sn*-1 and the polyunsaturated *sn*-2 chains, which crosses over between $n = 14$ and $n = 16$. It follows that the chain packing at the bilayer center is qualitatively different for the members of the homologous series.

In addition to altering the bilayer structure, substitution of the polyunsaturated DHA chain at position *sn*-2 also leads to a decreased cooperativity of the main phase transition, as shown by both ^{2}H NMR[34] and Raman spectroscopy.[62] Furthermore, the magnitude of the effect is found to differ for the various *sn*-1 saturated acyl lengths. Specifically, the case of 12 carbon acyl chains ($n_C = 12$) is close to an intersection point between the melting curve of the disaturated and mixed-chain DHA lipids and shows the largest hysteresis between cooling and heating melting temperatures. By contrast, the $n_C = 18$ lipids show the largest reduction of melting temperature upon unsaturation and

(60) Huber, T.; Rajamoorthi, K.; Kurze, V. F.; Beyer, K.; Brown, M. F. *J. Am. Chem. Soc.*, in press.
(61) Sun, W.-J.; Tristram-Nagle, S.; Suter, R. M.; Nagle, J. F. *Biophys. J.* **1996**, *71*, 885−891.
(62) Litman, B. J.; Lewis, E. N.; Levine, I. W. *Biochemistry* **1991**, *30*, 313−319.

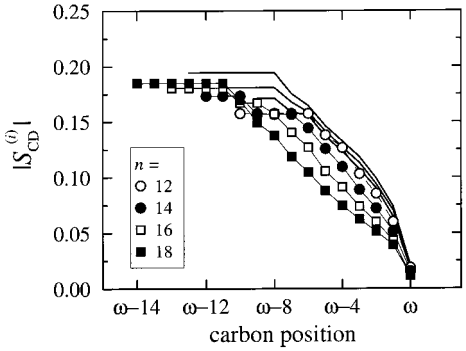

Figure 8. Comparison of order profiles of mixed-chain, polyunsaturated (n:0-d_{2n-1})(22:6)PC lipids (symbols) with disaturated di(m:0-d_{2m-1})PC lipids (solid lines) at $T = 50$ °C for chain lengths n_C ($\equiv m$ or n) between 12 and 18 carbons. The C$-^2$H bond order parameters are plotted as a function of reverse carbon number, ending with the ω carbon (terminal methyl). Note that for the disaturated lipids, the nonplateau segments essentially trace a common curve. In addition, the (12:0-d_{27})(22:6)PC data fall on this common saturated curve. However, the order profiles for the other mixed-chain, polyunsaturated lipids show a dramatic change of shape, viz. curvature, as the length of the *sn*-1 chain increases. (Similar behavior is observed at other temperatures.)

minimal hysteresis. How can we interpret these systematic variations in the context of the new findings reported here?

In Figure 8, we plot the ^{2}H NMR order parameter profiles for both the disaturated and the mixed-chain polyunsaturated series at 50 °C in reverse order; viz., all curves are shifted to coincide at the ω-carbon. (Note that di(18:0)PC is not in the fluid state at this temperature, and it is therefore not included.) Plotted this way, the experimental data facilitate a direct, model-free comparison of the two homologous series. As can be seen, the order profiles for the end acyl segments of the disaturated series trace a common curve, from which the polyunsaturated series deviates progressively for longer *sn*-1 chains. One can conclude that the different *sn*-1 saturated acyl chains pack qualitatively differently with the adjacent *sn*-2 DHA chain. The $n = 12$ profile nearly coincides with the disaturated profile, while the $n = 18$ case shows the largest deviation. In agreement with this result, Holte et al.[25] found that addition of three or more double bonds into the *sn*-2 chain significantly changed the order profile of the 18:0-d_{35} *sn*-1 chain, and that the change was not homogeneous along the chain. Here we show that the conclusion is valid for the whole (n:0)(22:6)PC series, and that the effect is progressively reduced for shorter *sn*-1 chains. Quite interestingly, one can still find a common characteristic feature for this series, as we show next.

Universal Chain Packing Curve for Mixed-Chain Polyunsaturated Phosphatidylcholines in the Fluid State. We shall now compare the disaturated and the polyunsaturated series by considering their acyl chain packing profiles, as explained below. The mean-torque model[35] used for calculation of the partial cross-sectional area per chain $\langle A_C^{(n:0)} \rangle$ can be used to determine average projections for *each* carbon segment (cf. Methods). The resulting segmental projections permit the calculation of average carbon positions, $\langle z^{(i)} \rangle$, relative to an arbitrary point chosen as reference. The resulting chain packing curves yield insight into the acyl chain geometry and facilitate direct comparison between different bilayer structures. We have previously shown[35] that, for the case of disaturated lipids, it is convenient to choose the methyl (ω) carbon as a reference and proceed along the chain toward the headgroup region. For convenience, the carbon atoms i are reindexed as $i' = n_C - i + c$, where c denotes an arbitrary

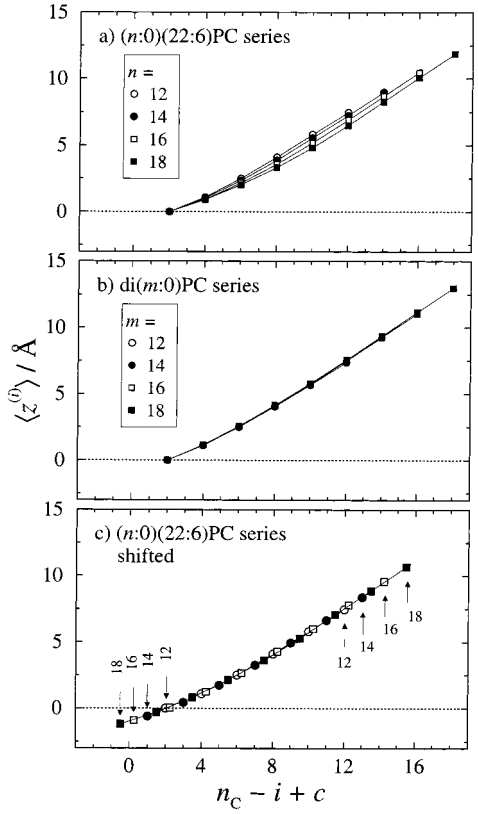

Figure 9. Mapping of ^{2}H NMR order profiles into chain packing curves, $\langle z^{(i)} \rangle$, obtained as a sum over acyl chain segmental projections onto the bilayer normal. (a) Saturated *sn*-1 chains of mixed-chain, polyunsaturated (n:0)(22:6)PC series at 50 °C. (b) Disaturated di(m:0)PC series at 65 °C. The curves $\langle z^{(i)} \rangle$ are plotted as a function of reverse carbon index $i' \equiv n_C - i + c$, where n_C denotes the chain length (m or n) and c is a relative shift. A value of $c = 2$ was chosen in parts a and b for all the lipids shown. In part c, the packing curves for the mixed-chain (n:0)(22:6)PC lipids are adjusted by shifting the individual curves along both the horizontal and the vertical axes. The resulting curve represents a universal packing profile for the saturated *sn*-1 acyl chain adjacent to a DHA chain at position *sn*-2. This clearly shows there is a midchain region of similar disorder (neutral volume) for all four mixed-chain, polyunsaturated lipids considered, with the longer saturated *sn*-1 chains having *increased* order toward the headgroup region and *decreased* order near the bilayer center.

shift value. For example, choosing $c = 2$ reverses the indexing, giving $i' = 2$ for the ω carbon and $i' = n_C$ for the C_2 carbon.

The chain packing profiles for the polyunsaturated series at 50 °C and the disaturated series at 65 °C are shown in Figure 9, parts a and b, respectively. (The value of $T = 65$ °C was selected for the disaturated series in order to have all four bilayers in the fluid state; similar behavior is seen at other temperatures.) From part a of Figure 9, it can be observed that the polyunsaturated series exhibits distinct packing profiles for each lipid, in contrast to the behavior of the disaturated lipids, which follow a common curve as shown in part b. For the saturated *sn*-1 chains, adjacent to a *sn*-2 DHA chain, part a, proceeding along the chain from the ω-carbon toward the lipid headgroup, the order increases less for longer chains. In parts a and b of Figure 9, a common value of $c = 2$ for the index shift was chosen for all lipids, such that all curves are coincident at the ω-carbon. With a closer inspection, one can find that all packing curves for the mixed-chain lipids in part a are actually sampled from a common profile, as shown in part c of Figure 9. Here, the curves from part a have been shifted along both axes, taking advantage of the fact that both the carbon average

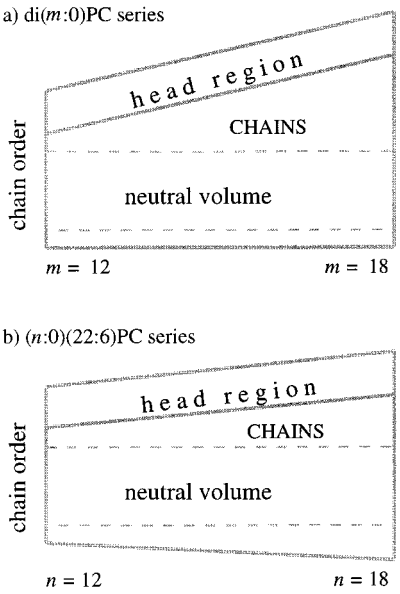

Figure 10. Schematic representation of saturated chain packing behavior of (a) disaturated di(*m*:0)PC series and (b) mixed-chain, polyunsaturated (*n*:0)(22:6)PC series as a function of *sn*-1 acyl length (*m* or *n*, respectively). The figure emphasizes the common midchain region (neutral volume), with increased order toward the lipid headgroup and increased disorder toward the chain ends near the bilayer center, as quantified by the chain packing curves shown in Figure 9. The universal chain packing curve, here depicted schematically, can be regarded as a continuous profile sampled discretely by individual saturated acyl chains. For the disaturated series (part a), more ordered states are sampled by longer acyl chains, while keeping the order at the bilayer center invariant. By contrast, the presence of DHA (part b) makes more disordered states accessible for the end segments, while reducing the accessibility to ordered states for the initial chain segments next to the headgroup.

position, $\langle z^{(i)} \rangle$, and the index number i' are relative quantities which depend linearly on the choice of a reference point. This result shows that, for the whole series, there is a region having a common degree of segmental order as for the disaturated series, but this region is shifted up along the chain, toward the headgroup, as the acyl length increases. In particular, at 50 °C, we find a shift of roughly one carbon for each two additional methylenes. The emerging chain packing curve can be viewed as a continuous profile that is sampled discretely by individual saturated acyl chains having different lengths.

These results suggest a picture of the saturated acyl chain packing within planar bilayers, as schematically diagrammed in Figure 10. As the length of the saturated *sn*-1 chain varies, there is a central (midchain) section, as delimited by the dashed horizontal lines in Figure 10, parts a and b. In this region, the acyl chain ordering and packing properties are largely conserved. This section of the bilayer can be regarded as a "neutral volume"; i.e., it is left invariant upon addition of methylene carbons to the saturated acyl chain. Outside of this region, the segmental order parameters change as a function of the acyl chain length, with a different variation for the disaturated versus the polyunsaturated series. For the like-chain disaturated phosphatidylcholines, part a, the acyl chain packing near the bilayer center changes very little with the addition of carbon segments, whereas the carbon segments next to the headgroups become more ordered. By contrast, for the mixed-chain, saturated−polyunsaturated phosphatidylcholines, part b, the end segments of the saturated chain become more disordered for longer acyl chains. An order increment of the carbon segments next to the headgroups is still present, albeit less pronounced than for the disaturated series. For both series, the variation with the acyl chain length follows a universal profile, as quantified by the chain packing profiles plotted in Figure 9.

Conclusions

We have shown that polyunsaturation at the glycerol *sn*-2 position affects the bilayer structure by comparing the homologous series of mixed-chain, saturated−polyunsaturated phosphatidylcholines with the corresponding disaturated series. A systematic analysis of the ^{2}H NMR data has revealed that the highly unsaturated DHA chains have significant disordering effects on the chain packing within the lipid bilayer, and that the magnitude of the effect increases progressively with increasing saturated acyl chain length. The variations across the series can be understood in terms of a universal, continuous chain packing curve characteristic of saturated acyl chains, which is sampled in discrete fashion by individual acyl chains. In all instances, DHA induces a loosening of the acyl chain packing, increasing the cross-sectional area per lipid headgroup as compared to disaturated bilayers. This disordering effect of DHA on the bilayer structure is expected to influence the interaction of the bilayer environment with proteins and membrane-bound peptides and, possibly, to modulate their biological functions.

Abbreviations

(12:0-d_{23})(22:6)PC, 1-perdeuteriolauroyl-2-docosahexaenoyl-*sn*-glycero-3-phosphocholine; (14:0-d_{27})(22:6)PC, 1-perdeuteriomyristoyl-2-docosahexaenoyl-*sn*-glycero-3-phosphocholine; (16:0-d_{31})(22:6)PC, 1-perdeuteriopalmitoyl-2-docosahexaenoyl-*sn*-glycero-3-phosphocholine; (18:0-d_{35})(22:6)PC, 1-perdeuteriostearoyl-2-docosahexaenoyl-*sn*-glycero-3-phosphocholine; di(12:0-d_{23})PC, 1,2-diperdeuteriolauroyl-*sn*-glycero-3-phosphocholine; di(14:0-d_{27})PC, 1,2-diperdeuteriomyristoyl-*sn*-glycero-3-phosphocholine; di(16:0-d_{31})PC, 1,2-diperdeuteriopalmitoyl-*sn*-glycero-3-phosphocholine; di(18:0-d_{35})PC, 1,2-diperdeuteriostearoyl-*sn*-glycero-3-phosphocholine; DHA, docosahexaenoic acid; DPA, docosapentaenoic acid; EFA, essential fatty acid; NMR, nuclear magnetic resonance; PC, phosphatidylcholine; PUFA, polyunsaturated fatty acid.

Acknowledgment. We thank Thomas Huber for many valuable discussions and critical reading of the manuscript. H.I.P. gratefully acknowledges Thomas B. Woolf for support and discussions related to this work. This research was supported by the U.S. National Institutes of Health and by the Röntgen-Professorship of Physics at the University of Würzburg.

JA011745N